

Article

MRCK α Is Dispensable for Breast Cancer Development in the MMTV-PyMT Model

Mei Qi Kwa ¹, Rafael Brandao ¹, Trong H. Phung ^{1,2}, Jianfeng Ge ^{1,3}, Giuseppe Scieri ¹ and Cord Brakebusch ^{1,*}

- ¹ Biotech Research and Innovation Center (BRIC), University of Copenhagen, Ole Maaløes vej 5, 2200 Copenhagen, Denmark; Kwa_Mei_Qi@sris.a-star.edu.sg (M.Q.K.); rafael.brandao@bric.ku.dk (R.B.); tphung@som.umaryland.edu (T.H.P.); gejianfeng1987@yahoo.com (J.G.); scieri.giuseppe@gmail.com (G.S.)
² Centre College, 600 W Walnut St, Danville, KY 40422, USA
³ Medical Research Centre (MRC) Cancer Unit, Hutchison/MRC Research Centre, University of Cambridge, P.O. Box 197, Biomedical Campus, Cambridge CB2 0XZ, UK
 * Correspondence: cord.brakebusch@bric.ku.dk

Abstract: MRCK α is a ubiquitously expressed serine/threonine kinase involved in cell contraction and F-actin turnover, which is highly amplified in human breast cancer and part of a gene expression signature for bad prognosis. Nothing is known about the in vivo function of MRCK α . To explore MRCK α function in development and in breast cancer, we generated mice lacking a functional MRCK α gene. Mice were born close to the Mendelian ratio and showed no obvious phenotype including a normal mammary gland formation. Assessing breast cancer development using the transgenic MMTV-PyMT mouse model, loss of MRCK α did not affect tumor onset, tumor growth and metastasis formation. Deleting MRCK α and its related family member MRCK β in two triple-negative breast cancer cell lines resulted in reduced invasion of MDA-MB-231 cells, but did not affect migration of 4T1 cells. Further genomic analysis of human breast cancers revealed that MRCK α is frequently co-amplified with the oncogenes ARID4B and AKT3 which might contribute to the prognostic value of MRCK α expression. Collectively, these data suggest that MRCK α might be a prognostic marker for breast cancer, but probably of limited functional importance.

Keywords: MRCK; breast cancer; invasion



Citation: Kwa, M.Q.; Brandao, R.; Phung, T.H.; Ge, J.; Scieri, G.; Brakebusch, C. MRCK α Is Dispensable for Breast Cancer Development in the MMTV-PyMT Model. *Cells* **2021**, *10*, 942. <https://doi.org/10.3390/cells10040942>

Academic Editor: Alexander E. Kalyuzhny

Received: 17 March 2021
 Accepted: 15 April 2021
 Published: 19 April 2021

Publisher's Note: MDPI stays neutral with regard to jurisdictional claims in published maps and institutional affiliations.



Copyright: © 2021 by the authors. Licensee MDPI, Basel, Switzerland. This article is an open access article distributed under the terms and conditions of the Creative Commons Attribution (CC BY) license (<https://creativecommons.org/licenses/by/4.0/>).

1. Introduction

Rho GTPases are small GTPases regulating the organization of the actin cytoskeleton and cell migration, but also differentiation, proliferation and other cellular processes [1]. They exert their function by binding and activating in their GTP bound form to effector molecules which then mediate the biological effects. The myotonic dystrophy kinase-related Cdc42-binding kinase α (MRCK α ; gene name *CDC42BPA*) is an effector of the ubiquitously expressed Rho GTPases Cdc42 and possibly Rac1 [2,3]. Binding of Cdc42 to MRCK α leads to autophosphorylation of MRCK α at S1003, which correlates with kinase activity [4]. Kinase activity is furthermore regulated by diacylglycerol binding to the centrally located C1 domain [5]. The MRCK α kinase domain is about 80% homologous to the kinase domain of MRCK β [6–8], and furthermore similar to the kinase domain of ROCK1/2, two closely related Rho effectors. This is believed to result in a shared set of substrates between MRCK α , MRCK β and ROCK1/2, including the regulatory subunits of the myosin light chain phosphatase (MYPT1) and of myosin II (MLC2) and the LIM kinases 1 and 2 [9]. Since phosphorylation of MYPT1 and MLC2 promotes cell contraction, while phosphorylation of the LIM kinases mediates inactivation of the F-actin severing cofilin, MRCK α is proposed to play an important role in the regulation of cell migration in collaboration with MRCK β , ROCK1 and ROCK2.

Indeed, several studies support an important role for MRCK α in cancer cell migration. In elongated MDA-MB-231 breast cancer cells, contraction and invasion into collagen or matrigel is jointly regulated by MRCK α , MRCK β , ROCK1 and ROCK2 [9,10]. Inhibition of either MRCK α/β or ROCK1/2 alone had only a partial effect. Invasion of the squamous cell carcinoma line SSC12 in an organotypic skin culture model, on the other hand, was largely dependent on MRCK α and MRCK β function [11]. In 2D migration, inhibition of both MRCKs by BDP9066 significantly reduced migration speed without affecting directionality [4]. However, MRCKs and ROCKs do not appear to always have overlapping effects. In neurite outgrowth assays in vitro, MRCK α is required for outgrowth, while ROCK1 promotes retraction [12]. Additionally, MRCK α/β are responsible for promoting SCC cell invasion through the matrix, whilst ROCK1/2 signaling contributes only in the leading fibroblasts to migration [11].

Little is known about the in vivo function of MRCK α during development and in disease, but several studies indicated a role for MRCK α in tumor formation. In DMBA/TPA induced skin tumor in mice, a strongly increased expression of MRCK α and MRCK β was observed [4]. Treatment with the MRCK inhibitor BDP9066 reduced the total tumor volume, but not the frequency of the papilloma, suggesting a role for MRCKs in tumor growth. This notion was supported by antiproliferative effects of BDP9066 on many cancer cell lines in vitro. In human breast cancer, MRCK α copy number was reported to be increased in 64% of 852 breast cancer samples at the Wellcome Trust Sanger Institute Cancer Genome Project [8]. Moreover, in a gene expression study of breast cancer patients, MRCK α , alias PK428, was identified as part of a profile of 70 genes predicting short interval to metastasis formation and poor prognosis [13]. These data suggest a potential role for MRCK α in breast cancer, although no validation analysis has been carried out.

To directly address the role of MRCK α in malignant breast cancer, we generated mice with a constitutive knockout of MRCK α using CRISPR genome editing and investigated their development and, by crossing with MMTV-PyMT mice, the formation of breast cancer. In addition, we tested redundancy of MRCK α and MRCK β in breast cancer cell lines in vitro. Our data reveal a dispensable role in MMTV-PyMT breast cancer model and cell type specific roles in 3D collagen gel invasion of breast cancer cells. In addition, we uncovered a co-amplification of MRCK α with two other known oncogenes in human cancers, which might contribute to the worse prognosis of breast cancer patients with amplified MRCK α .

2. Materials and Methods

2.1. Generation of MRCK α Ko Mice and Mammary Cancer Model

MRCK α KO mice were generated by the Transgenic Mouse Core Facility, University of Copenhagen, by direct injection of Cas9 mRNA and a guide RNA targeting exon 1 of mouse MRCK α (5'-TGTCCGGAGAAGTGCCTTTG AGG) to zygotes. The PAM sequence is underlined. Injected zygotes were embryo-transferred and mice born were genotyped by sequencing of the amplified target region. KO mice investigated in this study were genotyped with following a touchdown PCR protocol. The PCR cycling conditions were: 95 °C for 3 min, a touchdown phase consisting of 10 cycles of 95 °C for 30 s, a temperature ramp from 63 °C to 58 °C for 45 s at 0.5 °C per cycle, 72 °C for 1 min and then a second phase consisting of 25 cycles of 95 °C for 30 s, 58 °C for 45 s, 72 °C for 1 min and a final extension step of 72 °C for 10 min.

For the spontaneous mammary tumour model, MMTV-PyMT MRCK α HET male mice were crossed with HET female. MMTV-PyMT HET and MMTV-PyMT KO mice were monitored daily and sacrificed once the total tumour volume reached 1000 mm³. All animal experiments were carried out following national and European animal welfare regulations and were approved by the Danish Board for Animal Experiments (2016-15-0201-00946).

2.2. Quantification of Lung Micrometastasis

The number of micrometastases was counted manually on fixed lungs by Hematoxylin-Eosin staining of 5 μm paraffin sections of the left lung. Three random sections at least 100 μm apart in distance in the tissue were used for quantification per sample.

2.3. Primary Mammary Tumor Organoids

Primary tumor organoids were isolated from mammary tumors as previously described [14,15]. Briefly, mammary tumors were harvested from mice reaching end-point, minced with a scalpel and digested for 1 h at 37 °C in a collagenase solution (DMEM/F12 containing 2 mg/mL collagenase, 2 mg/mL trypsin, 5% FBS, 5 $\mu\text{g}/\text{mL}$ insulin and 50 $\mu\text{g}/\text{mL}$ gentamicin). The suspension was centrifuged at 500 $\times g$ for 10 min and the supernatant was carefully removed. The pellet was resuspended in warm DMEM/F12 media containing 1 U/ μL DNase I and incubated for 5 min. The suspension was then filtered through a 100 μm cell strainer and then pulse-centrifuged at 500 $\times g$ to remove the supernatant which contains fibroblasts. The pulse-centrifuging step was repeated a total of 4 times, or until the supernatant runs clear. The final pellet was resuspended in organoid culture media (DMEM/F12 containing 1% penicillin/streptomycin, 1% insulin-transferrin selenium and 2.5 nM human fibroblast growth factor basic) prior to being embedded in collagen I matrix.

2.4. Carmine Alum and Nissl Staining

For mammary gland branching analysis, 4th inguinal mammary fat pads were prepared as whole mount samples and carmine alum staining was performed according to the protocol as previously described [16]. For the analysis of brain sections, sagittal brain sections at 5 μm thickness were stained in 0.5% cresyl violet solution containing 3% glacial acetic acid, according to standard procedures for Nissl staining.

2.5. Cell Lines

Human MDA-MB-231 and murine 4T1 cells (both obtained by J. Erler, BRIC, University of Copenhagen). Immortalized mouse cancer associated fibroblasts were isolated from wildtype MMTV-PyMT tumors and immortalized by retroviral transduction of HPV-E6 29 [17]. CAFs were cultured in low-glucose DMEM containing 10% fetal bovine serum, 1% penicillin/streptomycin (Thermo Fisher Scientific, Lillerød, Denmark and 1% Insulin-Transferrin-Selenium (ITS-G) from Gibco. Cells were treated as indicated with 10 μM Y-27632 or 1 μM latrunculin (both Tocris, Abingdon, UK). All cell cultures were maintained at 37 °C, 5% CO₂.

2.6. Lentiviral Transduction

Single guide RNAs (sgRNA) targeting human MRCK α and MRCK β coding regions were designed and cloned into the lentiviral vector lentiCRISPRv2 (GeCKO; Addgene, Watertown, MA, USA) according to manufacturer's instructions. The oligonucleotide sequences corresponding to the human sgRNAs used were:

hMRCK α guide 1: F: 5' CACCGGCGGGCCCGCTCAGACCAA, R:5' AAAGTTGGTCTGAGCGGGCCCGCC

hMRCK α guide 2 F: 5' CACCGGAAGTGCGTTTGAGGCAGT, R:5' AAACACTGCCTCAAACGCACTTCC

hMRCK β guide 1 F: 5' CACCGGGCGGCACCATGTCCGCCA, R:5' AAAGTTGGCCGACATGGTGCCGCC

hMRCK β guide 2 F: 5' CACCAGGGCGCTCTCGTTGCGCCA, R:5' AAAGTTGGCGCAACGAGAGCGCCCT

The oligonucleotide sequences corresponding to the mouse sgRNAs used were:

mMRCK α guide 1: F: 5' CACCGGGTCCGGAGAAGTGCGTTTG, R:5' AAACCAAACGCACTTCTCCGGACCC

mMRCKa guide 2 F: 5' CACCGGAAGTGCCTTTGAGGCAGT, R:5' AAACACTGCCT-CAAACGCACTTC
hMRCKb guide 1 F: 5' CACCGGGGGCGGAGTTCCTCGAGTG, R:5' AAACCACTCGAG-GAACTCCGCCCC

Since no obvious differences were observed between ko cells generated with guide 1 or guide 2, results obtained with different guides for the same gene were pooled.

To produce viral particles, HEK293T cells were transfected with lentiviral vectors following standard procedures and viral supernatant was used to infect target cell lines. Selection was done using either puromycin (1–2 µg/mL) or blasticidin (8–10 µg/mL), 48 h post-transduction. An empty vector was transduced into cells as control.

2.7. Cell Adhesion

A 96-well tissue culture plate was coated for 1 h at room temperature using type I rat tail collagen serially diluted in PBS starting from 10 µg/mL to 0.00064 µg/mL. After coating, the plate was washed three times with PBS and then blocked in 1% BSA for 1 h. The plate was washed again for three times in PBS and cells are then seeded in serum-free media at a density of 2×10^4 cells per well and allowed to adhere. After 30 min of incubation at 37 °C, the plate was washed one time with PBS and the cells were given complete media and incubated at 37 °C for 3 h. The cells were fixed in 4% PFA for 20 min at room temperature and then stained in crystal violet diluted in 20% methanol for 15 min. After washing in PBS and then water, the plate was dried and the stain was extracted by 1% SDS in PBS. The extracted dye was transferred to a 96 well plate and absorbance at 560 nm was then read from the plate.

2.8. Cell Proliferation Assay

Cells were seeded at a density of 7×10^3 per well in a 12 well plate format. After overnight incubation, the cells were placed in the Incucyte system for live cell imaging and automated quantification. An image was taken every 2 h, for a total of 48 h.

2.9. F and G Actin Fractionation

For fractionation of the F and G actin cells were lysed in actin stabilization lysis buffer (50 mM PIPES, 50 mM NaCl, 5 mM MgCl₂, 5 mM EGTA, 2 mM ATP, 5% glycerol, 0.1% Nonidet P-40, 0.1% Triton X-100, 0.1% Tween 20, 0.1% β-mercaptoethanol, protease inhibitors and phosphatase inhibitors) for 10 min at 37 °C. Cell debris were removed by centrifugation at $300 \times g$ and protein concentration of the supernatant was determined. After equilibrating the protein concentration of the samples using the lysis buffer, an aliquot of the lysate (10% of total volume) was stored as total protein input, while the remainder was subjected to ultracentrifugation at $100,000 \times g$ for 1 h at 37 °C. After centrifugation, the supernatant containing G actin was carefully transferred to a new tube and stored, while the pellet containing F actin was resuspended in cold lysis buffer containing 1 µM cytochalasin D and incubated on ice for 45 min to dissolve the fibers into monomers. All fractions were then boiled in Laemmli buffer and prepared for Western blotting.

2.10. Western Blot Analysis

Tissue fragments and cultured cells were lysed with Laemmli buffer. Lysates were separated by a 10% SDS-PAGE and Western blotting was carried out following standard protocols. For detection, the following primary antibodies were used: MRCKα (#374568), MRCKβ (#374597), GAPDH (#25778; all SantaCruz Biotechnology, Dallas, TX, USA), pMLC (#3674), pCofilin (#3311; all Cell Signaling, Danvers, MA, USA), β actin (#AB6276, Abcam, Cambridge, MA, USA). For detection, appropriate HRP coupled secondary antibodies were used: horse-anti-mouse IgG (#VECTPI2000), goat-anti-rabbit IgG (#VECTPI1000, all Vector Laboratories, Burlingame, CA, USA). Luminata™ Western HRP Chemiluminescence Substrates detection reagent (Milipore, Hellerup, Denmark) was used for chemilumines-

cence, which was then detected with Medical X-ray film (AGFA, Birkerød, Denmark). The intensity of the bands was quantified using ImageJ software.

2.11. *D Spheroid Invasion Assay*

Spheroids were generated from aggregated cells, either homogeneously or heterogeneously in combination with CAF [17]. Briefly, 500 cancer cells (with or without 500 CAFs) were seeded into 96 well round bottom plates containing 20% methylcellulose in serum-free DMEM. After overnight incubation at 37 °C and 5% CO₂, the aggregated spheroids were embedded in 2 mg/mL collagen I (Corning, Glendale, AZ, USA) in 12-well plates at approximately 10 spheroids per well. After polymerization, the collagen matrix was overlaid with 500 µL of DMEM containing 2% FBS and, when indicated, 10 µg/mL Y-27632 (Sigma Aldrich, St. Louis, MO, USA). The spheroids were imaged immediately after overlaying with media to obtain the initial area of the core spheroid and again after 24 h incubation. Phase contrast images were captured using an Olympus CellSens imaging software.

2.12. *Spheroid Image Quantification*

For quantification, images were analyzed using Fiji/ImageJ [18,19]. Spheroid area measurements were determined semi-automatically using a custom macro on ImageJ. First, images were smoothed by applying a Gaussian blur filter with a sigma of 2. Next, the spheroid was outlined by manual thresholding. Gaps in the spheroids were filled with the Fill Hole command and the total area of the spheroid was then measured. The area of the spheroid imaged at 24 h post-embedding was subtracted from that obtained at 0 h, to obtain the final area of the invasion zone.

2.13. *Time-Lapse Microscopy*

5×10^3 MDA-MB-231 cells stably expressing a LifeACT-GFP plasmid (Addgene, Warrington, MA, USA) were seeded in 8-well chambered glass slides. 24 h post-incubation, the cells were then imaged by time-lapsed microscopy on a DeltaVision suite Olympus microscope. Images were captured every 5 s for a total of 10 min, under a 40× magnification using immersion oil. Kymographs were generated as described previously using ImageJ [20]. Briefly, a line was first drawn from the middle of the cell perpendicularly towards the migrating front of cells. Then, the Reslice function was used to generate the kymograph. A new line was again drawn along each actin protrusion on the kymograph and the enclosed triangle, of which each dimension corresponds to the protrusion length (P), persistence (S) and protrusion rate (P/S), were then measured in pixel units. All lines are indicated in the corresponding figure.

2.14. *RNA-Sequencing and Data Analysis*

Total RNA was isolated from vector control, MRCK α KO, MRCK β KO or DKO MDA-MB-231 cells using standard RNA purification kit (Sigma-Aldrich, St. Louis, MO, USA). For DKO samples, 2 different sets were generated using the guide 1 or the guide 2 gRNAs for hMRCK α or hMRCK β . Two sets of control samples were obtained from two separate transductions of the vector plasmid. RNA sequencing was performed by the Beijing Genomics Institute (BGI). Sequencing depth was at least 10 M clean reads per sample via SE50. To compare the differential gene expression, the FPKM values obtained from the analysis performed by BGI were used. For the control and DKO samples, FPKM values from both transductions (vector) or both gRNA sets (DKO) were first compared and FPKM of genes that differed by more than 2-fold were excluded from subsequent analysis. An average is obtained from the remaining genes. Log₂ fold-change was then calculated for the MRCK α KO, MRCK β KO and DKO samples against vector control. An arbitrary log₂ fold change of 1 (and -1) was used as threshold for differential expression.

2.15. Statistics

Data are presented as means with error bars representing standard error of the mean. Statistical significance was determined by the two-tailed Student's *t*-test, if not indicated otherwise. For all statistical analyses, *p* values are denoted as: *** $p < 0.001$, ** $p < 0.01$ and * $p < 0.05$.

3. Results

3.1. MRCK α Expression Correlates with Survival in Triple-Negative Breast Cancer

MRCK α expression has been reported to be increased in breast cancer. Indeed, around 11% of the breast cancers of the TCGA breast cancer data set (cbioportal.org) [21,22] showed genetic alterations of the MRCK α gene, most of them amplifications (Figure 1a). The closely related MRCK β gene was only altered in 2.6%, including both amplifications and homozygous deletions (Figure 1a). Further investigating the patients with amplifications of the MRCK α gene, we observed a trend towards reduced progression free survival, suggesting that amplification of the MRCK α gene might be disease relevant ($p = 0.087$; Figure 1b). Amplifications of the MRCK α gene were observed in Basal, Her2+, Luminal A, Luminal B and Normal breast cancers, but were enriched in the Basal subgroup (Figure 1c). Average expression of MRCK α in the amplified subset was increased by about 21% compared to the non-amplified subset ($p = 0.015$). In contrast, increased expression of MRCK β showed no obvious effect on breast cancer survival and cancers with high expression of MRCK β were strongly depleted in the Basal subset (Supplementary Figure S1). These data suggest that MRCK α expression might be of relevance for breast cancer formation and progression in all subtypes, but probably most in Basal Cancer.

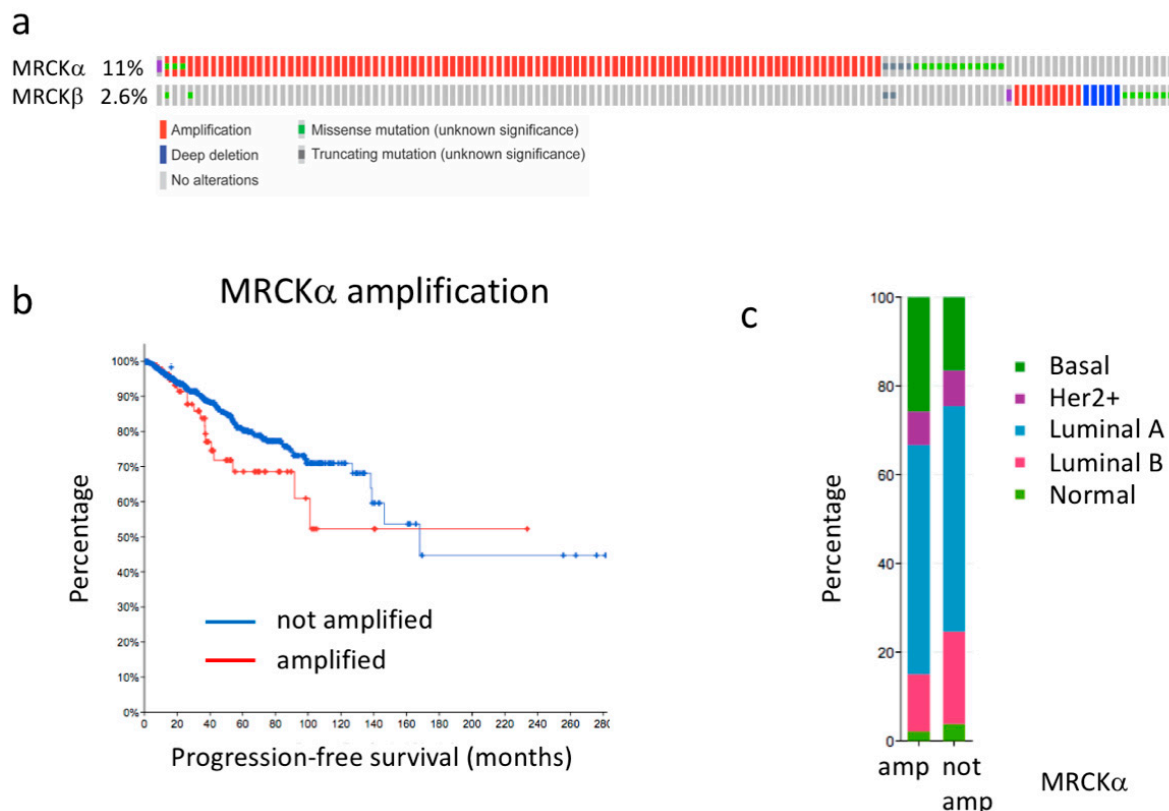


Figure 1. MRCK α gene is amplified in breast cancer. (a) Genetic alterations of the MRCK α and MRCK β genes in breast cancer. (b) Progression free survival of breast cancer patients with amplified and non-amplified MRCK α gene ($p = 0.087$). (c) Breast cancer subtype distribution of patients with amplified (amp) and not amplified (not amp) MRCK α gene. All graphs were generated in cBioPortal.org using the TCGA PanCancer Atlas data set for invasive breast carcinoma (accessed on 20 March 2021).

3.2. MRCK α Ko Mice Do Not Show an Obvious Phenotype

To analyze the requirement of MRCK α for breast cancer, we first generated mice lacking a functional MRCK α gene (Cdc42bpa) using CRISPR genome editing. Several MRCK α mutant mouse lines were generated and the p.Leu7fs*35 line (KO) in which an extra “T” was introduced into the leucine 7 codon (Figure 2a) was chosen for further analysis.

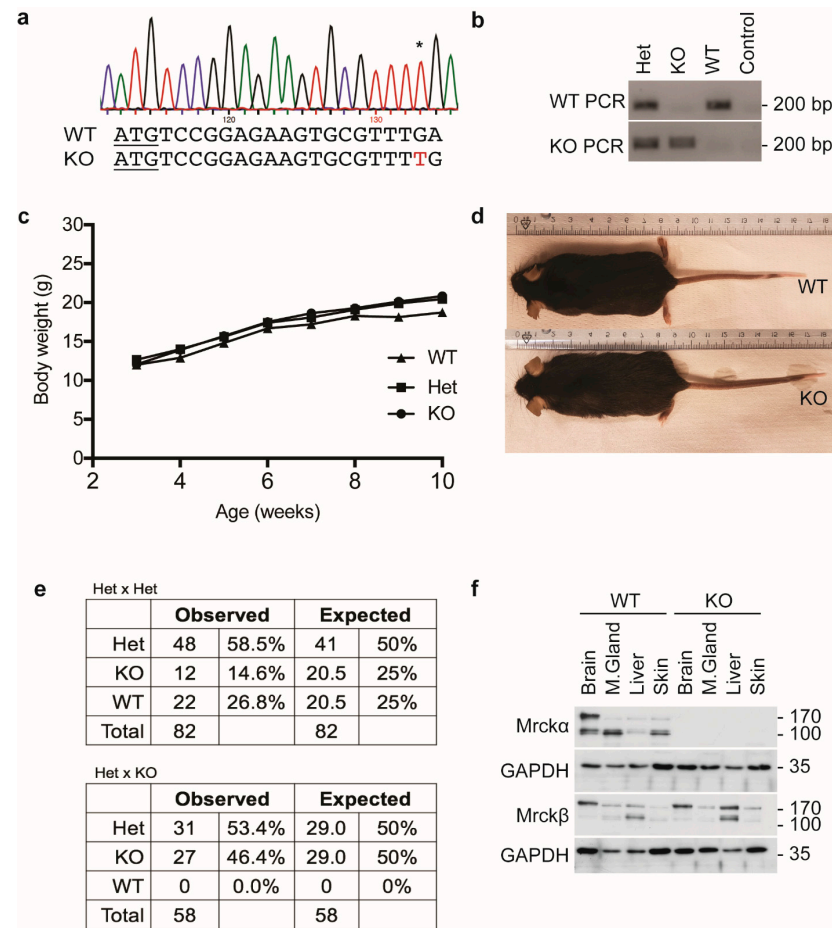


Figure 2. MRCK α ko mice show no obvious phenotype. (a) Genotype profile of ko mice showing the p.Leu7fs*35 mutation. * indicates the inserted nucleotide in the chromatogram. (b) Representative results from genotyping PCR using primers targeting the mutation specifically. (c) Body weight measurements of post-weaning female wild-type, heterozygous and ko mice. (d) Representative images of wild-type and ko mice. (e) Mendelian ratio of the observed and expected frequencies of wild-type, heterozygous and ko mice in Het \times Het mating ($n = 82$) and Het \times KO ($n = 58$) mating pairs. (f) Immunoblot analysis of MRCK α and MRCK β expression in wild-type and ko mice.

Homozygous KO mice developed without obvious defects and showed normal size and body weight (Figure 2b–d). Cage behavior (explorative activity, body posture, culling) was indistinguishable from control litter mates (wildtype, heterozygous) and both male and female ko mice were fertile. Crosses of heterozygous mice (Het), showed a slight reduction of KO mice compared to the expected level (Figure 2e). However, checking embryonic litters at different time points before birth no evidence for prenatal lethality or morphological defects could be found (data not shown). Moreover, crosses of KO and Het were born roughly at the Mendelian ratio, giving no indication for partial embryonic lethality (Figure 2e).

To confirm the loss of MRCK α on protein level, lysates of brain, mammary gland, liver and skin were analyzed by Western blotting. WT mice showed that, in addition to the expected isoform of about 190 kD corresponding to the full-length MRCK α , smaller isoforms of about 130 kD were detectable. In brain, larger and smaller isoforms were

equally expressed, while in the other tissues the smaller isoform was dominant (Figure 2f). Both isoforms were not detectable in KO mice, indicating efficient gene deletion and specificity of the antibody. The closely related MRCK β was also expressed in different isoforms in all tissues tested. In addition, liver, the high molecular weight isoform was more prevalent (Figure 2f). Loss of MRCK α did not result in increased protein levels of MRCK β in the tissues investigated.

Since MRCK α was highly expressed in brain and in mammary gland we assessed both tissues for histological changes in the KO mice. However, Nissl staining of sagittal brain sections (Figure 3a) revealed no obvious alterations. Histological analysis of the mammary gland by hematoxylin/eosin staining indicated normal ducts surrounded by a thin layer of connective tissue in both WT and KO (Figure 3b). Moreover, whole mount staining by carmine alum indicated normal branching morphogenesis of the mammary ducts in MRCK α KO mice (Figure 3c,d).

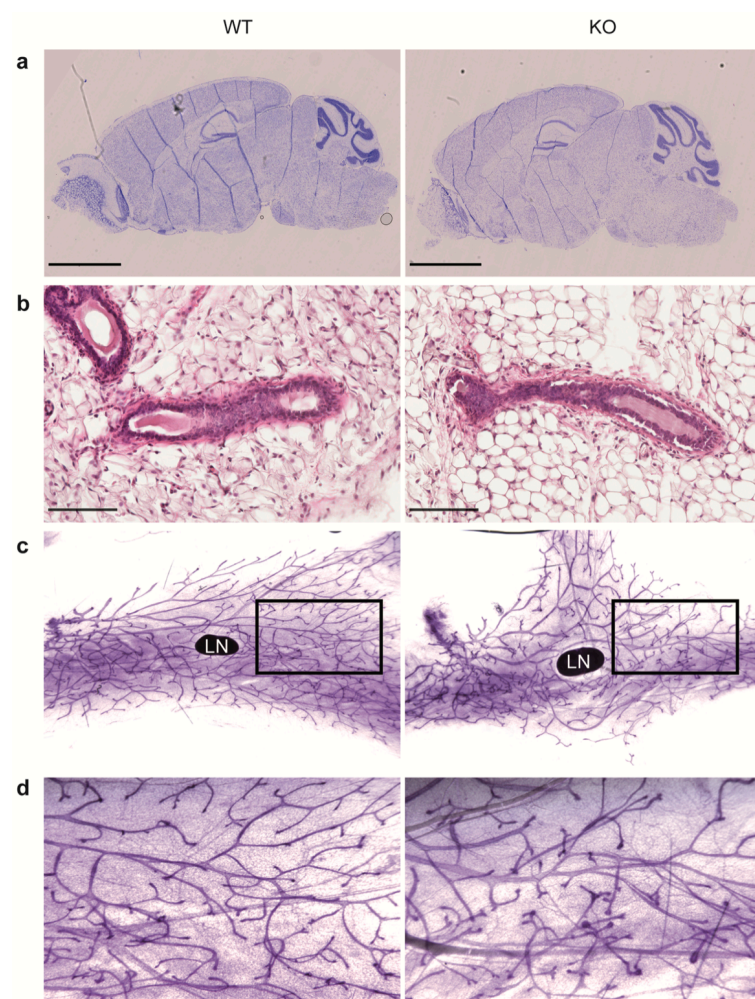


Figure 3. Mrck α knockout does not affect brain and mammary gland development. (a) Representative Nissl staining of sagittal brain sections from adult wild-type and ko mice. Scale bars: 2.5 mm. (b) Representative H&E staining of the 4th inguinal mammary glands from 7-weeks old virgin female wild-type and KO mice. Scale bars: 100 μ m. (c) Representative carmine alum-stained mammary gland whole mounts. LN denotes the inguinal lymph node. A black box was drawn to indicate the area of magnification of the image, as shown in (d).

These data reveal that MRCK α is not required for development. Importantly, the normal development of the mammary gland and the normal overall phenotype provides an excellent basis for the analysis of the role of MRCK α in breast cancer development, since a potential tumor phenotype will not be affected by a developmental phenotype.

3.3. MRCK α Is Not Essential for Tumorigenesis or Metastasis in the Mmtv-PyMT Breast Cancer Model

To investigate the role of MRCK α in breast cancer in an in vivo model, we crossed the MRCK α KO mice with MMTV-PyMT mice, which spontaneously develop invasive ductal breast carcinoma with metastases in the lung [23].

Surprisingly, loss of MRCK α did not affect the tumor onset, tumor-free survival and tumor volume (Figure 4a–c). Histological analysis of tumors in KO and Het control mice indicated adenocarcinoma characterized by increased size of nuclei, nuclear pleomorphism, prominent nucleoli and areas of necrosis in more advanced carcinoma (Figure 4d). Occasional infiltration of mononuclear cells and desmoplasia were observed. Tumors appeared relatively solid without single cells or small groups of cells detached from the main tumor. Western blot analysis of tumors confirmed the lack of MRCK α and showed no clear compensatory upregulation of MRCK β (Supplementary Figure S2a). In one of 6 KO tumors, MRCK α expression was even decreased. Frequency and histology of lung metastases was similar in Het and KO mice (Figure 4e,f).

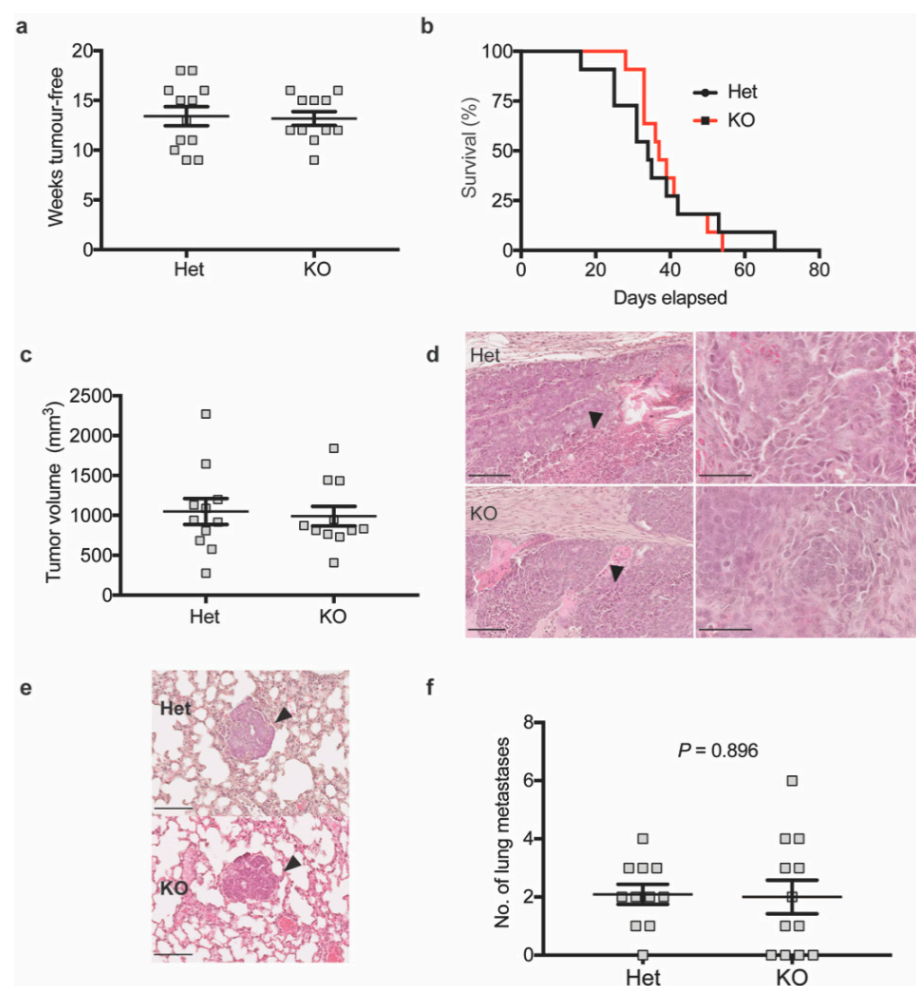


Figure 4. Mrck α knockout does not affect primary mammary tumour development and metastasis in MMTV-PyMT mice. (a) Weeks tumour-free (b) survival analysis ($p = 0.8243$, log-rank test) and (c) tumor volume at end-point of MMTV-PyMT heterozygous (Het) vs. KO mice ($n \geq 10/10$). (d) Representative H&E staining of MMTV-PyMT heterozygous or Mrck α KO mice primary tumours showing extensive necrosis (black arrows). Images on the right represent the same images at higher magnification showing the abnormal cancer cell nuclei. Scale bars: 100 μm . (e) Representative H&E staining of lung metastases of MMTV-PyMT heterozygous vs. KO mice. Scale bars: 100 μm . (f) Quantitation of lung metastases by counting of foci from the left lung lobe from MMTV-PyMT heterozygous and KO mice upon reaching end point. ($n: 10/10$; mean \pm SEM, two-tailed unpaired t -test).

To identify qualitative changes in the invasion process, we monitored breast cancer invasion in tumor organoids embedded in collagen. Collective cell migration of cancer cells into the collagen gel was detected in both Het and KO cancers without any apparent alterations in KO tumor organoids (Supplementary Figure S1b). These data suggest that MRCK α is not essential for breast cancer development, progression and lung metastasis in the MMTV-PyMT model.

3.4. MRCK α Is Important for 3D Collagen Gel Invasion of MDA-MB-231 Breast Cancer Cells

The unaltered breast cancer development in MRCK α ko mice could be related to functional redundancy of MRCK α with MRCK β . To investigate this possibility, we deleted the genes for MRCK α and MRCK β individually or alone in two breast cancer cell lines. Since it was shown earlier that siRNA mediated knockdown of MRCK α and MRCK β together reduces matrigel invasion of the triple-negative breast cancer cell line MDA-MB-231 [9], we chose this cell line for the experiments.

MDA-MB-231 breast cancer cells lacking MRCK α , MRCK β , or both (DKO) were established by lentiviral CRISPR genome editing and selection for stably transduced cells. As a control, MDA-MB-231 cells were transduced with the empty vector. Control MDA-MB-231 cells expressed primarily the high molecular weight isoforms of MRCK α and MRCK β (Figure 5a). Even without clone picking, the efficiency of gene deletion was very high as tested on protein level (Figure 5a–c). Interestingly, KO of MRCK α resulted in a slight but significant increase in MRCK β expression. On the other hand, loss of MRCK β did not affect MRCK α protein levels to a significant extent.

Next, invasion of spheroid aggregates of the different MDA-MB-231 breast cancer cell lines mixed with CAFs into 3D collagen gels was assessed. Initially, all spheroids were relatively compact and of similar diameter, although some cells were already detached from the main cell mass at 0 h (Figure 5d; Supplementary Videos S1 and S2). Reproducibly, the number of detached cells at 0 h was lower for DKO than for WT, suggesting reduced invasiveness (Supplementary Videos S1 and S2). For the quantification, only the differences between 24 h and 0 h was taken into consideration (Figure 5d).

After 24 h, MRCK α KO spheroids showed significantly less invasion than control cells (Figure 5e,f). DKO spheroids also showed defective 3D migration, while MRCK β KO spheroids were indistinguishable from controls. Movies demonstrated that both control and DKO cells invaded the collagen gel mostly in a rounded and less frequently in an elongated form (Supplementary Videos S1 and S2).

These data indicate a role for MRCK α in the collagen invasion of MDA-MB-231 breast cancer cells, but not for MRCK β .

3.5. Subtle Cellular and Biochemical Alterations in Mutant MDA-MB-231 Cells Cultured in 2D

To identify cellular and biochemical alterations of the MDA-MB-231 cells with mutations in MRCK genes, we investigated the breast cancer cells in 2D culture. MRCK single and double KO cells were morphologically similar to control MDA-MB-231, with a slightly elongated cell shape (Figure 6a). Assessing proliferation in a confluency assay, KO lines and control cells showed a similar growth rate (Figure 6b). Furthermore, adhesion to collagen was identical in all cells (Figure 6c), suggesting that integrin mediated collagen binding is not changed by loss of MRCK.

To study dynamic changes in F-actin formation and protrusions at the plasma membrane, we transfected the cells with the fluorescent F-actin marker LifeAct and monitored F-actin by time lapse fluorescence microscopy. In randomly chosen sections through lamellipodial regions, distance, persistence and rate of protrusions was measured by kymograph analysis (Figure 6d–f). Distance of protrusions was slightly higher in MRCK α KO and lower in DKO, suggesting that loss of MRCK α and MRCK β results in subtle changes in actin cytoskeleton dynamics (Figure 6g–i).

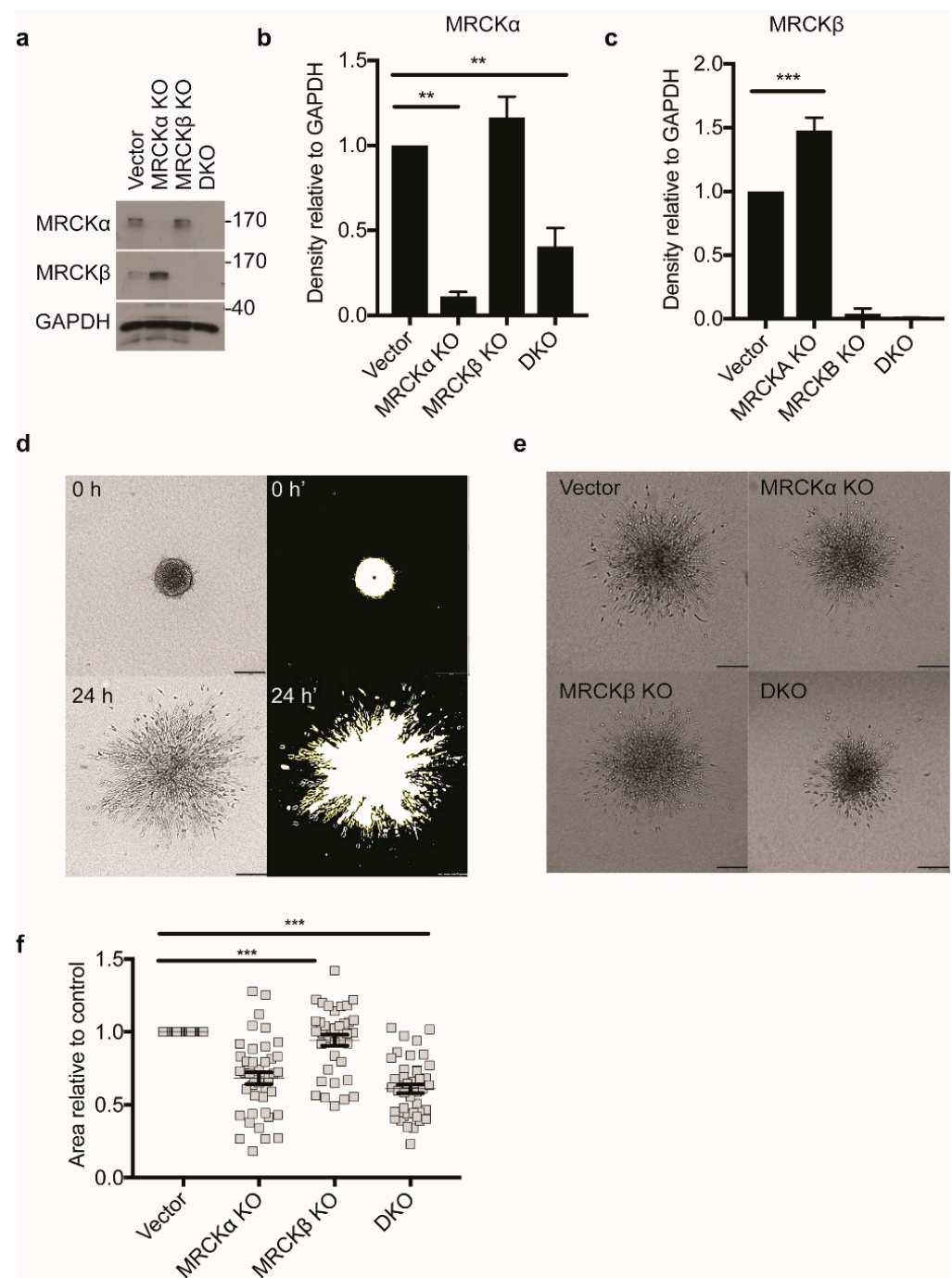


Figure 5. MRCK α and MRCK β knockout affect 3D invasion. (a) Representative immunoblot showing successful MRCK α and MRCK β , single and double knockout (DKO) in MDA-MB-231 cells. Quantitation of (b) MRCK α and (c) MRCK β expression in lysates relative to GAPDH ($n = 3$, mean \pm SEM, one-way ANOVA; ** $p \leq 0.01$; *** $p \leq 0.001$). (d) Strategy for quantifying area of invasion of spheroids by thresholding using ImageJ. Briefly, area of spheroids immediately after embedding in type I collagen was subtracted from the total area of the same spheroids 24 h post-embedding, to obtain the area of invasion (e) 3D matrix invasion of vector control, MRCK α KO, MRCK β KO, or DKO MDA-MB-231 heterospheroids co-cultured with CAFs and embedded in type I collagen. Scale bar: 200 μ m. (f) Area of collagen invasion relative to vector control ($n = 3$, totaling > than 100 cells per group; mean \pm SEM, one-way ANOVA; *** $p \leq 0.001$).

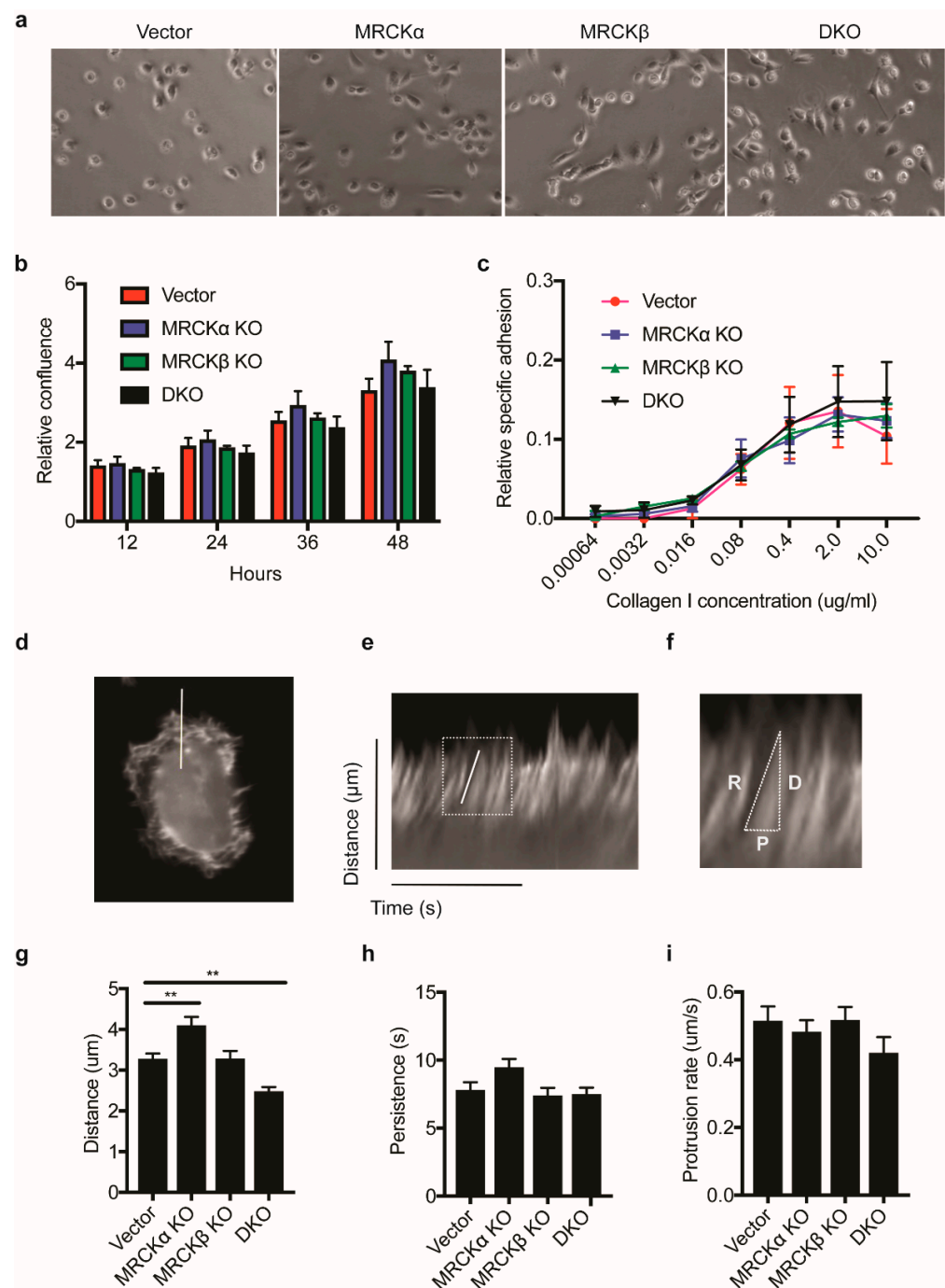


Figure 6. MRCK KO has a modest effect on F-actin polymerization. (a) Representative phase contrast images showing the morphologies of control, MRCK α KO, MRCK β KO, or DKO MDA-MB-231 cells (b) Proliferation rate of MRCK α KO, MRCK β KO and DKO MDA-MB-231 cells as measured by relative confluency over time. (c) Relative adhesion of MRCK α KO, MRCK β KO and DKO MDA-MB-231 cells to increasing concentration of type I collagen. Data is obtained for 3 biological replicates. (d–i) Kymograph analysis of actin protrusion distance, rate and persistence in MRCK KO cells (d) Representative still image of an MDA-MB-231 cell expressing LifeAct-GFP used in live imaging. A white line was drawn perpendicular to the cell body to indicate the position where kymograph was obtained. (e) Example of a kymograph generated using the reslice function on ImageJ program, showing the distance and time in the y and x axis, respectively. A white box is used to highlight an actin protrusion and the image magnified in (f). (f) Example of a measurement of actin protrusion distance, D , persistence, P and protrusion rate, R . (g) Kymograph measurements obtained for protrusion distance, $** p \leq 0.01$ (h) persistence and (i) protrusion rate.

Earlier, MRCK α and MRCK β were shown to regulate together with ROCK the phosphorylation of cofilin and myosin light chain (MLC), corresponding to increased F-actin formation and increased cell contraction. Unexpectedly, in our MDA-MB-231 cells neither in MRCK α KO nor in MRCK β KO a decrease in pMLC, pCofilin, or F-actin was detectable (Figure 7a–e). They rather appeared to be increased in MRCK α KO MDA-MB-231 cells, although the differences were not significant. DKO cells showed slightly reduced pMLC compared to vector transfected controls.

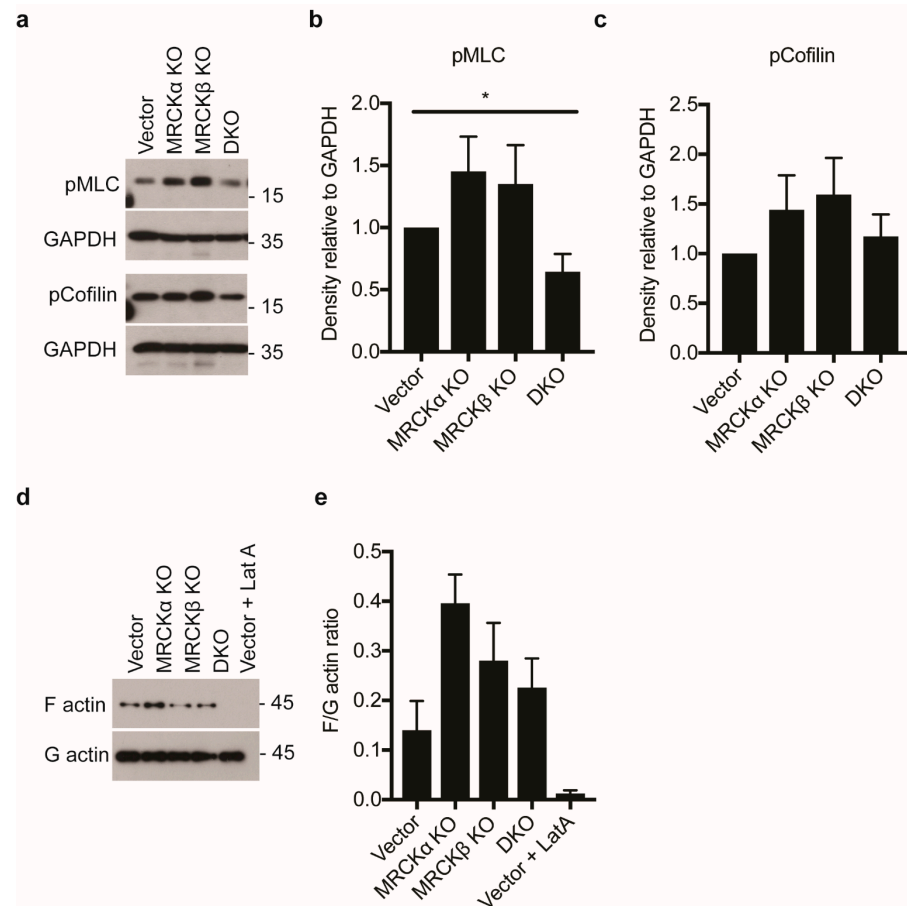


Figure 7. MRCK KO does not effectively reduce myosin and cofilin phosphorylation in MDA-MB-231 cells (a) Representative immunoblot showing myosin light chain (pMLC) and phospho-cofilin in MDA-MB-231 cells with MRCK α KO, MRCK β KO, or DKO. (b,c) Quantitation of indicated proteins from lysates obtained from the knockout cells (n : 6/6/6/6; mean \pm SEM, one-way ANOVA; * $p \leq 0.05$). (d) Representative immunoblot showing levels of F-actin and G-actin in control, MRCK α KO, MRCK β KO and DKO MDA-MB-231 cells. As a control, cells were also treated with 1 μ M latrunculin A (Lat A) for 15 min. (e) Quantification of F/G-actin ratio (n : 6/6/6/6; mean \pm SEM, not significant with one-way ANOVA, * $p \leq 0.05$ with two-tailed t -test for Vector vs. MRCK α KO).

We then tested for differential gene expression by RNA sequencing, excluding poorly expressed genes. Functional annotation of the differentially regulated genes by DAVID suggested a coordinated regulation of immune response related genes in the DKO and the MRCK α KO cells, with no obvious indication of any alterations in pathways related to cell migration (Supplementary Figures S3–S5). The lists of top up- and down-regulated genes in the MRCK KO cells can be found as Supplementary Tables S1–S6). Within the lists, none of the genes altered more than 2-fold was obviously related to actin cytoskeletal regulation or cell migration, besides the actin nucleator LMOD1 [24], which was upregulated in MRCK β KO cells, but neither in MRCK α KO nor in DKO cells. This suggests that MRCK α and MRCK β regulate cell migration mainly at posttranscriptional level. Taken together, MRCK α KO and DKO cells display small changes in 2D culture compared to control cells.

3.6. Collective 3D Invasion of 4T1 Breast Cancer Is Not Dependent on MRCK α

MDA-MB-231 cells invade collagen gels mostly as single cells, while the tumor organoids of MRCK α KO and control breast cancers only showed collective migration (Supplementary Figure S1b). To test the function of MRCK α and MRCK β in 3D collagen gel invasion assays also with triple-negative breast cancer cells showing collective migration, we performed additional experiments with murine 4T1 cells. CRISPR genome editing resulted in efficient deletion of MRCK α and MRCK β protein as tested by Western blot (Figure 8a). As was the case for MDA-MB-231 cells, MRCK α KO cells have increased MRCK β expression, although the reverse was not consistently observed (Supplementary Figure S6a,b). Control, KO and DKO cells showed similar morphology and were both growing in colonies, suggesting strong cell-cell interactions (Figure 8b). In 3D collagen gel invasion assays, 4T1 cells displayed collective migration similar to the organoids isolated from the MMTV-PyMT mice (Figure 8c,d). However, neither deletion of MRCK α or MRCK β or both reduced the invasion significantly.

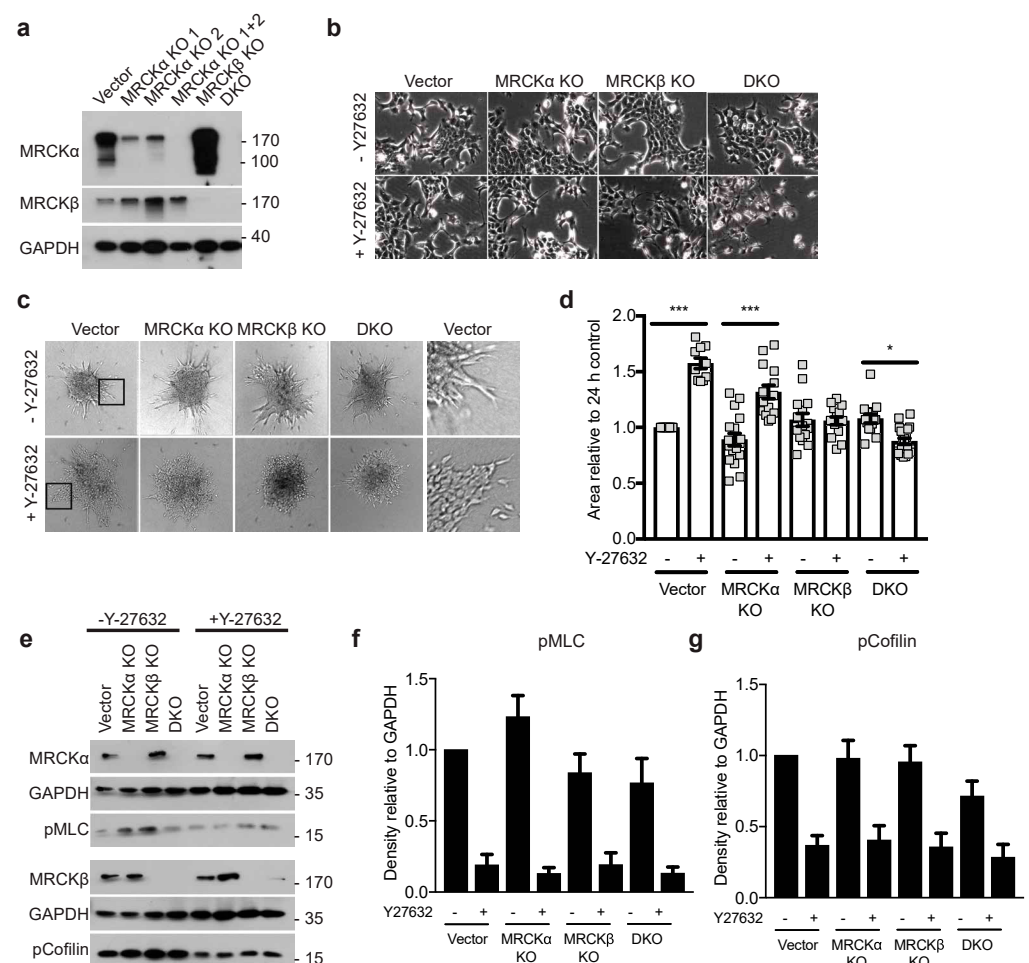


Figure 8. MRCK α and MRCK β are dispensable in 4T1 cells matrix invasion. (a) Representative immunoblot showing successful knockout of MRCK α and MRCK β in 4T1 cells. DKO was achieved by using one of two different CRISPR gRNAs for MRCK α (“MRCK α 1 + 2”) and one gRNA for MRCK β (b) Representative phase contrast images of control, MRCK α , MRCK β and DKO 4T1 cell morphologies in the presence and absence of Y-27632 (10 μ M). (c) 3D matrix invasion of MRCK KO 4T1 spheroids in type I collagen, in the presence and absence of Y-27632 (10 μ M). Black boxes highlight the invasion front of the control spheroids, as shown magnified in the right panel. (d) Quantification of the area of invasion of the 4T1 spheroids from (c) relative to 24 h control ($n = 3$; mean \pm SEM, one-way ANOVA; * $p < 0.05$, *** $p < 0.001$). (e) Representative immunoblot and (f,g) quantification of the expression of the indicated proteins. ($n = 5$; mean \pm SEM, one-way ANOVA).

Previously, it had been shown that inhibition of ROCK1 and ROCK2, in addition to MRCK α and MRCK β strongly impaired migration of cancer cells [9,10]. We therefore repeated the collagen invasion assay in the presence of Y-27632, which efficiently inhibits ROCK1 and ROCK2. Unexpectedly, however, Y-27632 increased the collagen invasion of 4T1 cells (Figure 8c,d). Deletion of MRCK α and even more of MRCK β blocked this increased invasion. DKO cells showed a reduced invasion when ROCK was inhibited. In the presence of Y-27632, cell-cell borders became clearly visible in all 4T1 lines in 3D, suggesting altered cell-cell contacts (Figure 8c). Still, cells appeared not to migrate as individual cells in contrast to MDA-MB-231 (Figure 5). In 2D, Y-27632 treated cells grew less in colonies and displayed thin and long plasma membrane protrusions (Figure 8b). Phosphorylated MLC (pMLC) and pCofilin were not significantly affected by the loss of MRCK α , MRCK β , or both (Figure 8e–g). These data suggest that inhibition of ROCK signaling promotes invasion of 4T1 breast cancer cells in an MRCK dependent manner, but a dispensable role for MRCK α and MRCK β in 4T1 cell for collective cell migration in 3D.

3.7. MRCK α Is Co-Amplified with the Oncogenes AKT3 and ARID4B in Breast Cancer

In cancer, some genes are amplified not because they are driver genes themselves but because they are co-amplified with an oncogene in the vicinity. We therefore, tested in breast cancers of the TCGA PanCancer dataset whether other amplified oncogenes are close to the chromosomal location of the MRCK α gene (Chr 1q41.13). Indeed, both ARID4B (Chr 1q42.3) and AKT3 (Chr 1q43-q44) are in the neighborhood of the MRCK α gene. ARID4B is an activator of the PI3K-AKT pathway, an oncogene in PTEN-deficient prostate cancer [25] and amplified in 12% of breast cancers in the TCGA data set. AKT3 showed an oncogenic effect in the murine MMTV-PyMT mammary cancer model [26]. Around 11% of human breast cancers show amplification of AKT3. Interestingly, ARID4B, MRCK α and AKT3 are mostly amplified together and show a highly significant co-occurrence of genetic alterations in breast cancer (Figure 9a,b).

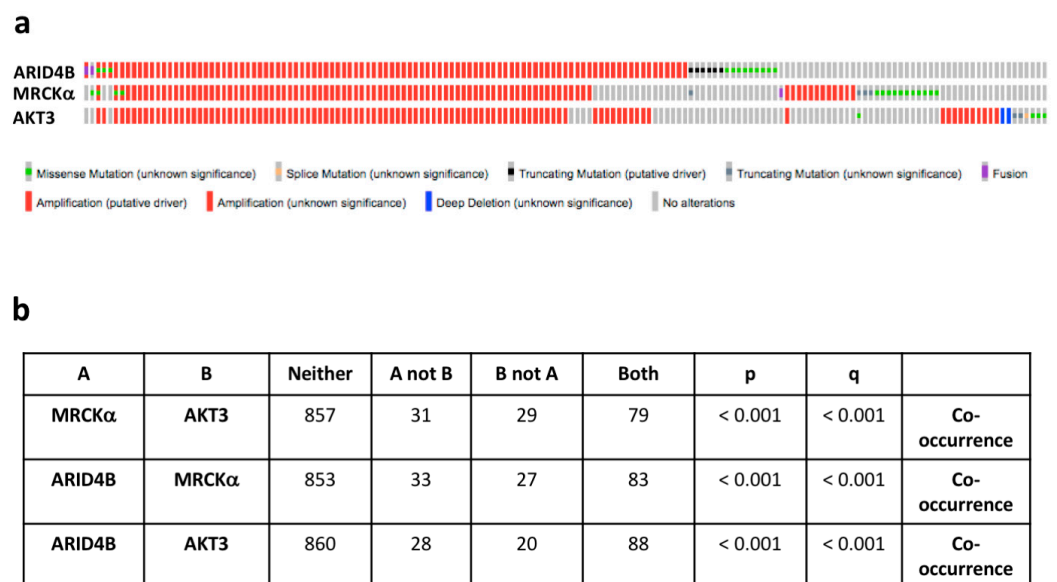


Figure 9. MRCK α is co-amplified with ARID4B and AKT3. (a) Oncoprints of genomic alterations of MRCK α , ARID4B and AKT3 in human breast cancers. (b) Analysis of co-occurrence of MRCK α with the oncogenes ARID4B and AKT3. All analyses were generated in cBioportal (TCGA PanCancer Atlas, breast cancer samples, accessed on 20 February 2021).

Importantly, patients with amplified ARID4B showed a significant decrease in disease-free survival ($p = 0.049$), in contrast to patients with amplified MRCK α ($p = 0.101$) and AKT3 ($p = 0.108$), despite the high overlap of the patient populations. Cancer with amplified ARID4B displayed a 29% increase in ARID4B expression, which was highly significant

(1.17×10^{-8}). AKT3 expression was similarly increased in cancers with AKT3 amplification, but with a much lower significance (28%; $p = 0.036$). Compared to amplifications of MRCK α and AKT3, amplifications of ARID4B showed the strongest enrichment in the Basal cancer subtype.

These statistical analyses of patient data suggest that ARID4B might have the strongest tumor promoting effect of the three co-amplified genes. Furthermore, the correlation of MRCK α expression with breast cancer formation and progression appears to be at least partly due to the co-amplification with AKT3 and in particular ARID4B.

4. Discussion

In order to study MRCK α function in breast cancer, we first established mice with a constitutive inactivation of the MRCK α gene in all cells. Previous *in vitro* studies suggested a role for MRCK α in developmental processes involving Cdc42 dependent cell migration and in neurite formation in the brain [12,27]. Analysis of our MRCK α KO mice did not reveal an obvious developmental function, which might be caused by redundant function of the closely related MRCK β gene.

Despite the genetic amplification of MRCK α in human breast cancers, we found that loss of MRCK α had no obvious effect on primary tumor growth in the murine MMTV-PyMT model. Since inhibition of MRCK α and MRCK β decreased papilloma volume in a DMBA/TPA induced skin tumor model [4], functional redundancy between MRCK α and MRCK β or tumor specific function could explain the normal growth of MRCK α KO breast cancers. Cell-type specific effect of MRCKs were already observed earlier when testing 757 cancer cell lines from 45 different tumors for their sensitivity to MRCK inhibitors [4]. Here, hematopoietic cancers showed growth inhibition at much lower doses than breast cancer cell lines. In this context, it should be noted that acute inhibition by small molecule inhibitors might result in different effects than chronic elimination of a protein, which could trigger compensatory mechanisms [28]. We tested for a compensatory effect of ROCK in 4T1 cells lacking MRCK α and MRCK β by treatment with the ROCK inhibitor Y27632, but did not observe it in this cell line.

MDA-MB-231 and 4T1 are triple negative breast cancer cell lines, which is similar to the Basal breast cell cancer subtype. The MMTV-PyMT breast cancer corresponds to the human Luminal B subtype [23]. However, more extensive experiments are required to test whether the findings can be extrapolated to all breast cancer subtypes.

An alternative explanation for the reported results is that MRCK α is a passenger gene that is co-amplified with ARID4B and AKT3, which have been reported to be driver genes in earlier studies, although no clinical studies have been carried out investigating their prognostic value. High expression of MRCK α could therefore correlate with a bad prognosis, although MRCK α itself might not be an oncogene.

Based on earlier studies, a role for MRCK α was expected in invasion and metastasis of breast cancer cells. Previously, it was shown that siRNA mediated inhibition of MRCK α and MRCK β in cancer cells reduced their invasion into collagen gel [10]. Similarly, simultaneous knockdown of MRCK α and MRCK β in MDA-MB-231 cells decreased their invasion into matrigel [9]. Moreover, collective migration of squamous cell carcinoma cells SSC12 in an organotypic culture system including fibroblasts was strongly reduced after knockdown of MRCK α and MRCK β [11]. In human breast cancer, MRCK α is amplified in many patients, correlating with early metastasis [13]. Indeed, we found that deleting the MRCK α gene either alone or together with MRCK β significantly reduced 3D collagen invasion of MDA-MB-231 cells. This altered invasion in 3D did not correlate with changes in pMLC or pCofilin in 2D culture, indicating either a different regulation of cell contraction (pMLC) and F-actin severing (pCofilin) in 3D vs. 2D or a different mechanism for MRCK α dependent invasion of MDA-MB-231 cells.

In the MMTV-PyMT breast cancer model, however, no significant reduction of lung metastases was observed in the absence of MRCK α . In contrast to MDA-MB-231 cells, cancer cells of the MMTV-PyMT model showed collective migration in collagen as tested with

tumor organoids, suggesting that the mode of migration might determine the importance of MRCK α in breast cancer. This notion is supported by the finding that MRCK α is not required for the 3D collagen invasion of the murine 4T1 breast cancer cell line, which also shows collective migration. Whether species specific differences contribute to the observed changes could not be determined.

Using a murine knockout model, the current study reveals that MRCK α is not essential for PyMT induced breast cancer. However, our results do not exclude that increased expression of MRCK α could promote breast cancer or exacerbate its progression.

Taken together, these data support further analysis of MRCK α expression as a possible prognostic marker, but do not validate MRCK α as a drug target in breast cancer, although it might play a role in a subset of cancers showing mesenchymal migration.

Supplementary Materials: The following are available online at <https://www.mdpi.com/article/10.3390/cells10040942/s1>. Supplementary legends. Figure S1: (a) Overall survival of breast cancer patients with high and low expression of MRCK β ($p = 0.899$). (e) Breast cancer subtype distribution of patients with high and low expression of MRCK β . Graphs were generated in cBioPortal.org using the TCGA PanCancer Atlas data set for invasive breast carcinoma (accessed on 20 March 2021). Figure S2: MRCK α knockout tumour organoids metastasize normally, Figure S3. RNA-seq analysis of MRCK α knockout cells, Figure S4. RNA-seq analysis of MRCK β knockout cells, Figure S5. RNA-seq analysis of MRCK DKO cell, Figure S6. MRCK α knockout in 4T1 cells results in MRCK β up-regulation, Video S1: Invasion of control MDA-MB-231 breast cancer cells into 3D collagen gel, Video S2: Invasion of MRCK α /MRCK β DKO MDA-MB-231 breast cancer cells into 3D collagen gel.

Author Contributions: M.Q.K. designed, executed and analysed experiments. R.B. designed and generated the MRCK α KO mice. G.S. generated the CAF cells. J.G. designed the targeting guide RNA for the 4T1 cells. T.H.P. carried out experiments. C.B. conceived the project, designed experiments. M.Q.K. and C.B. wrote the manuscript. All authors have read and agreed to the published version of the manuscript.

Funding: This project has received funding from the European Union's Horizon 2020 research and innovation programme under the Marie Skłodowska-Curie grant agreement No 703589.

Institutional Review Board Statement: The animal experiments were approved by the Danish Board for Animal Experiments (2016-15-0201-00946).

Informed Consent Statement: Not applicable.

Data Availability Statement: The data that supports the findings of this study are available in the figures and the supplementary material of this article. RNAseq data are available at the Gene Expression Omnibus (GEO) database (<https://www.ncbi.nlm.nih.gov/geo/>), under the accession number GSE169000.

Acknowledgments: We thank Volkan Turan for excellent technical help.

Conflicts of Interest: The authors declare no conflict of interest. The funders had no role in the design of the study; in the collection, analyses, or interpretation of data; in the writing of the manuscript, or in the decision to publish the results.

References

1. Lawson, C.D.; Ridley, A.J. Rho GTPase signaling complexes in cell migration and invasion. *J. Cell Biol.* **2018**, *217*, 447–457. [[CrossRef](#)] [[PubMed](#)]
2. Leung, T.; Chen, X.Q.; Tan, I.; Manser, E.; Lim, L. Myotonic dystrophy kinase-related Cdc42-binding kinase acts as a Cdc42 effector in promoting cytoskeletal reorganization. *Mol. Cell Biol.* **1998**, *18*, 130–140. [[CrossRef](#)]
3. Schwarz, J.; Proff, J.; Hävemeier, A.; Ladwein, M.; Rottner, K.; Barlag, B.; Pich, A.; Tatge, H.; Just, I.; Gerhard, R. Serine-71 phosphorylation of Rac1 modulates downstream signaling. *PLoS ONE* **2012**, *7*, e44358.
4. Unbekandt, M.; Belshaw, S.; Bower, J.; Clarke, M.; Cordes, J.; Crighton, D.; Croft, D.R.; Drysdale, M.J.; Garnett, M.J.; Gill, K.; et al. Discovery of Potent and Selective MRCK Inhibitors with Therapeutic Effect on Skin Cancer. *Cancer Res.* **2018**, *78*, 2096–2114. [[CrossRef](#)]
5. Tan, I.; Seow, K.T.; Lim, L.; Leung, T. Intermolecular and intramolecular interactions regulate catalytic activity of myotonic dystrophy kinase-related Cdc42-binding kinase alpha. *Mol. Cell Biol.* **2001**, *21*, 2767–2778. [[CrossRef](#)] [[PubMed](#)]

6. Moncrieff, C.L.; Bailey, M.E.; Morrison, N.; Johnson, K.J. Cloning and chromosomal localization of human Cdc42-binding protein kinase beta. *Genomics* **1999**, *57*, 297–300. [[CrossRef](#)]
7. Tan, I.; Cheong, A.; Lim, L.; Leung, T. Genomic organization of human myotonic dystrophy kinase-related Cdc42-binding kinase alpha reveals multiple alternative splicing and functional diversity. *Gene* **2003**, *304*, 107–115. [[CrossRef](#)]
8. Unbekandt, M.; Olson, M.F. The actin-myosin regulatory MRCK kinases: Regulation, biological functions and associations with human cancer. *J. Mol. Med.* **2014**, *92*, 217–225. [[CrossRef](#)] [[PubMed](#)]
9. Heikkila, T.; Wheatley, E.; Crighton, D.; Schroder, E.; Boakes, A.; Kaye, S.J.; Mezna, M.; Pang, L.; Rushbrooke, M.; Turnbull, A.; et al. Co-crystal structures of inhibitors with MRCKbeta, a key regulator of tumor cell invasion. *PLoS ONE* **2011**, *6*, e24825. [[CrossRef](#)]
10. Wilkinson, S.; Paterson, H.F.; Marshall, C.J. Cdc42-MRCK and Rho-ROCK signalling cooperate in myosin phosphorylation and cell invasion. *Nat. Cell Biol.* **2005**, *7*, 255–261. [[CrossRef](#)]
11. Gaggioli, C.; Hooper, S.; Hidalgo-Carcedo, C.; Grosse, R.; Marshall, J.F.; Harrington, K.; Sahai, E. Fibroblast-led collective invasion of carcinoma cells with differing roles for RhoGTPases in leading and following cells. *Nat. Cell Biol.* **2007**, *9*, 1392–1400. [[CrossRef](#)]
12. Chen, X.Q.; Tan, I.; Leung, T.; Lim, L. The myotonic dystrophy kinase-related Cdc42-binding kinase is involved in the regulation of neurite outgrowth in PC12 cells. *J. Biol. Chem.* **1999**, *274*, 19901–19905. [[CrossRef](#)]
13. Van't Veer, L.J.; Dai, H.; Van De Vijver, M.J.; He, Y.D.; Hart, A.A.; Mao, M.; Peterse, H.L.; van der Kooy, K.; Marton, M.J.; Witteveen, A.T.; et al. Gene expression profiling predicts clinical outcome of breast cancer. *Nature* **2002**, *415*, 530–536. [[CrossRef](#)] [[PubMed](#)]
14. Cheung, K.J.; Gabrielson, E.; Werb, Z.; Ewald, A.J. Collective invasion in breast cancer re-quires a conserved basal epithelial program. *Cell* **2013**, *155*, 1639–1651. [[CrossRef](#)] [[PubMed](#)]
15. Diermeier, S.D.; Spector, D.L. Antisense Oligonucleotide-mediated Knockdown in Mam-mary Tumor Organoids. *Bio Protoc.* **2017**, *7*, e2511. [[CrossRef](#)] [[PubMed](#)]
16. Robinson, G.W.; Hennighausen, L. Inhibins and activins regulate mammary epithelial cell differentiation through mesenchymal-epithelial interactions. *Development* **1997**, *124*, 2701–2708.
17. Calvo, F.; Ege, N.; Grande-Garcia, A.; Hooper, S.; Jenkins, R.P.; Chaudhry, S.I.; Harrington, K.; Williamson, P.; Moeendarbary, E.; Charras, G.; et al. Mechanotransduction and YAP-dependent matrix remodelling is required for the generation and maintenance of cancer-associated fibroblasts. *Nat. Cell Biol.* **2013**, *15*, 637–646. [[CrossRef](#)]
18. Schindelin, J.; Arganda-Carreras, I.; Frise, E.; Kaynig, V.; Longair, M.; Pietzsch, T.; Preibisch, S.; Rueden, C.; Saalfeld, S.; Schmid, B.; et al. Fiji: An open-source platform for biological-image analysis. *Nat. Methods* **2012**, *9*, 676–682. [[CrossRef](#)]
19. Schneider, C.A.; Rasband, W.S.; Eliceiri, K.W. NIH Image to ImageJ: 25 years of image analysis. *Nat. Methods* **2012**, *9*, 671–675. [[CrossRef](#)]
20. Doggett, T.M.; Breslin, J.W. Study of the actin cytoskeleton in live endothelial cells ex-pressing GFP-actin. *J. Vis. Exp.* **2011**, *57*, 3187.
21. Cerami, E.; Gao, J.; Dogrusoz, U.; Gross, B.E.; Sumer, S.O.; Aksoy, B.A.; Jacobsen, A.; Byrne, C.J.; Heuer, M.L.; Larsson, E.; et al. The cBio cancer genomics portal: An open platform for exploring multidimensional cancer genomics data. *Cancer Discov.* **2012**, *2*, 401–404. [[CrossRef](#)]
22. Gao, J.; Aksoy, B.A.; Dogrusoz, U.; Dresdner, G.; Gross, B.; Sumer, S.O.; Sun, Y.; Jacobsen, A.; Sinha, R.; Larsson, E.; et al. Integrative analysis of complex cancer genomics and clinical profiles using the cBioPortal. *Sci. Signal.* **2013**, *6*, 11. [[CrossRef](#)] [[PubMed](#)]
23. Attalla, S.; Taifour, T.; Bui, T.; Muller, W. Insights from transgenic mouse models of PyMT-induced breast cancer: Re-capitulating human breast cancer progression in vivo. *Oncogene* **2021**, *40*, 475–491. [[CrossRef](#)] [[PubMed](#)]
24. Chereau, D.; Boczkowska, M.; Skwarek-Maruszewska, A.; Fujiwara, I.; Hayes, D.B.; Rebowski, G.; Lappalainen, P.; Pollard, T.D.; Dominguez, R. Leiomodin is an actin filament nucleator in muscle cells. *Science* **2008**, *320*, 239–243. [[CrossRef](#)] [[PubMed](#)]
25. Wu, R.C.; Young, I.C.; Chen, Y.F.; Chuang, S.T.; Toubaji, A.; Wu, M.Y. Identification of the PTEN-ARID4B-PI3K pathway reveals the dependency on ARID4B by PTEN-deficient prostate cancer. *Nat. Commun.* **2019**, *10*, 4332. [[CrossRef](#)] [[PubMed](#)]
26. Maroulakou, I.G.; Oemler, W.; Naber, S.P.; Tschlis, P.N. Akt1 ablation inhibits, whereas Akt2 ablation accelerates, the development of mammary adenocarcinomas in mouse mammary tumor virus (MMTV)-ErbB2/neu and MMTV-polyoma middle T transgenic mice. *Cancer Res.* **2007**, *67*, 167–177. [[CrossRef](#)]
27. Kale, V.P.; Hengst, J.A.; Desai, D.H.; Amin, S.G.; Yun, J.K. The regulatory roles of ROCK and MRCK kinases in the plasticity of cancer cell migration. *Cancer Lett.* **2015**, *361*, 185–196. [[CrossRef](#)]
28. Cerikan, B.; Shaheen, R.; Colo, G.P.; Gläßer, C.; Hata, S.; Knobloch, K.P.; Alkuraya, F.S.; Fässler, R.; Schiebel, E. Cell-Intrinsic Adaptation Arising from Chronic Ablation of a Key Rho GTPase Regulator. *Dev. Cell* **2016**, *39*, 28–43. [[CrossRef](#)]